IEEE Access
Multidisciplinary | Rapid Review | Open Access Journal

Received August 5, 2019, accepted August 20, 2019, date of publication August 27, 2019, date of current version September 12, 2019.

Digital Object Identifier 10.1109/ACCESS.2019.2937808

Synthesis and Use of Bio-Based Dielectric Substrate for Implanted Radio Frequency Antennas

AUSTIN TESSER[1], ALA ALEMARYEEN[2], JEREMY LEWIS[1], ALI ALSHAMI[1], MEYSAM HAGHSHENAS[3], AND SIMA NOGHANIAN[4], (Senior Member, IEEE)

[1]Department of Chemical Engineering, University of North Dakota, Grand Forks, ND 58202, USA
[2]School of Electrical Engineering and Computer Science, University of North Dakota, Grand Forks, ND 58202, USA
[3]Department of Mechanical Engineering, University of North Dakota, Grand Forks, ND 58202, USA
[4]Phoenix Analysis and Design Technologies (PADT) Inc., Tempe, AZ 85284, USA

Corresponding author: Ali Alshami (ali.alshami@und.edu)

This work was supported in part by the North Dakota Established Program to Stimulate Competitive Research (ND EPSCoR) under Grant FAR0023660.

ABSTRACT Equipped with precision sensors/antenna modules combined with integrated processing and telemetry circuitry, wireless implants that are both biocompatible and biodegradable are important devices for monitoring patient's conditions and patient's safety. In this article we report on the development, design, and testing of a bio-based monopole radio frequency (RF) sensor/antenna module for potential use in human health applications. The module is built on a dielectric substrate biocomposite made of 0.5:1.0 ratio of polylactic acid (PLA) to sunflower carbon substrate (SCS) produced via pyrolysis of seeds shells. Findings for the SCS include optimized reactor yields around 7.9 wt.% at 500°C, a 0.27:1.0 fixed to elemental carbon content, dielectric constant near 3.4, loss factor between 0.0 and 0.4 measured in the 1 to 6 GHz frequency range. The PLA-SCS biocomposite exhibited comparable dielectric properties to those of pure SCS, a 17% elastic modulus increase, and over 500% increase in hardness. Numerical simulation of the designed sensor/antenna module agreed fairly well with the experimental validation results. Tests of the fabricated sensor/antenna module on water, soil and muscle tissue phantom, as well as implanted inside muscle tissue phantom, via the reflection coefficient (S_{11}) and in a communication link via the transmission coefficient (S_{21}) confirmed use and applicability of the developed antenna.

INDEX TERMS Monopole antenna, bio-based substrate, pyrolysis, polylactic acid composite.

I. INTRODUCTION

Biodegradable electronics have made tremendous impacts on human society and has been widely used in almost every field, including telecommunication, entertainment, and healthcare. A comprehensive material database including semiconductor, dielectric, metal, and encapsulation materials is of crucial importance for the construction of biodegradable electronics. In general, demonstrated biodegradable devices are categorized into fully degradable and partially degradable devices based upon the used materials and the intended application.

Applications of such devices in the healthcare field include implantable drug delivery systems with programmable release [1], bioresorbable silicon electronics for transient spatiotemporal mapping of electrical activity from the cerebral cortex [2], and bioresorbable intracranial sensors adapted to sense fluid flow, motion, pH or thermal characteristics [3].

The wireless implants provide a wireless link for transferring information. The data link can be through an inductive link. The inductive link works based on low frequency magnetic coupling. This type of coupling is very efficient for small distances, but as the distance increases the efficiency drops significantly. To establish a wireless link at larger distances radio frequency (RF) is required. Therefore, biodegradable RF devices are of particular significance. These devices have been gaining momentum and have become a major focus of research and development efforts due to principally critical characteristics including improving health, monitoring patient's conditions and patient's safety. Biocompatible and biodegradable devices are engineered to completely resorb in the human body after fulfilling their therapeutic and diagnostic functions, thereby

The associate editor coordinating the review of this article and approving it for publication was Mingchun Tang.

avoiding secondary procedures to remove the implants after their period of use [4], [5]. Equipped with precision sensors/antenna modules combined with integrated processing and telemetry circuitry, wireless implants can remotely monitor a variety of physical and chemical parameters within the human body, and thereby allow an immediate evaluation of an individual's medical conditions.

Some of the examples of implanted technology used in biomedical devices include cardiac pacemakers and defibrillators [6], [7], visual prosthetic device (a devices that can create visual sensation) [8], brain computer interface (a method of interpreting neural brain signals and transferring them to a device) [9], ingestible electronic pills (a devices for gastrointestinal (GI) tract or reporting, or other medical observations), and wireless capsule endoscopy, also known as video capsule endoscopy (VCE) [10]. For a good review of the implanted wireless devices please see [11].

In [12] a single use biodegradable pressure sensor is proposed for cardiovascular monitoring. The sensor consists of a flexible capacitor. The substrate is a laminate of poly (glycerolsebacate) (PGS) in the center and polyhydroxyvalerate (PHB/PHV) on top and bottom. The conductive layers of Magnesium (Mg) and Iron (Fe) are located between PGS and PHB/PHV.

Another example is given in [13] where a wireless RF Micro-Electro-Mechanical Systems (MEMS) pressure sensor made entirely of biodegradable materials is presented. The sensor consists of a cavity, bounded by two conductors to form a capacitor, connected to an inductor coil. The inductor is used as a part of a sensor as well as a part of magnetically coupling the sensor to the external coil. Biodegradable polymers poly(L-lactide) (PLLA) and polycaprolactone (PCL) were used as the substrate and bonding and sealing materials. Zinc (Zn) and Fe combination was used for the conducting layers.

Antenna is the fundamental RF building block of the wireless communication of the implantable devices. Planar antennas have been used as a part of wireless sensors in multiple applications. For example in [14] a wireless temperature sensor is proposed based on a scattering antenna as a part of passive radio frequency identification (RFID) systems that consists of a meandered microstrip line and an ultrawideband monopole antenna. In [15] a temperature sensor is designed based on a microstrip patch antenna as a scattering antenna. Planar antennas require two types of materials: dielectric, and conductive materials. Since we are interested in biocompatible materials the choices should be of materials that have this characteristics. For the conductive part, Mg and Fe and their alloys are known to be biodegradable and are already being used in bio-implants. There are also biodegradable conductive polymer composites such as polymers poly (L-lactide) PLLA–polypyrrole (PPy) and polycaprolactone (PCL–PPy). The widely used polymers such as biodegradable polymers PLLA and PCL can be used as substrate.

Various planar biocompatible and some biodegradable antennas can be found in the literature. In [16] an implantable CPW fed monopole U slot antenna is designed using RT Duroid substrate for the Industrial scientific medical (ISM) band of 2.4 GHz – 2.5GHz. Several planar antennas are proposed [17] for implanting in human brain. These antennas were designed and fabricated using Kapton polyimide substrate for the flexible antennas and Al_2O_3 for the rigid antennas. The antennas were designed 2 GHz – 11 GHz range substrate with a thickness to cover both ISM and ultra-wideband (UWB) bands. The above examples were examples of planar biocompatible antennas. There are limited number publications on the biodegradable antennas. For example in [18] polybutylene succinate (PBS) substrate is used in a co-planar waveguide (CPW) fed planar monopole, working at 1.78 GHz to 2.80 GHz to be used for ISM band. PBS is known to be biodegradable polymer. Dr. John Rogers has demonstrate several examples of biocompatible and biodegradable sensors and antennas. In [19] an example of energy harvesting system that harvest RF energy and transmits signal via a wireless link is shown. The construction of this circuit included two sodium carboxymethylcellulose (Na-CMC) substrates with electrical connections made of biodegradable metals such as magnesium (Mg), tungsten (W), and/or zinc (Zn). A layer of poly(ethylene oxide) (PEO) between the Na-CMC films were used for connecting them. The system was a temperature sensor transmitting data at 2.47 GHz – 2.49 GHz. PEO and Na-CMC are water soluble and biocompatible. The same paper presents two loop antennas on NA-CMC working at 1.04GHz. In [20] the same group presented wireless passive antennas used for food quality monitoring at different frequency ranges. The antennas were made on silk substrate.

The antenna design for implanted devices imposes some special challenges. The antenna needs to radiate through body tissue and surroundings that usually have very high dielectric properties that can vary from point to point. Therefore, a loading effect is present that can change the antenna's resonance frequency. A narrowband antenna can be detuned due to these changes in the dielectric properties. To mitigate this effect usually UWB antennas are preferred. UWB antennas maintain their frequency bandwidth of operation [21]. UWB signals are transmitted in the unlicensed federal communications commission (FCC) approved frequency range of 3.1-10.6 GHz. It is worth mentioning that UWB systems offer several advantages over the conventional narrowband systems such as higher data-rates, lower power consumption leads to a longer battery life, smaller antennas, and less complexity on the transmitter side [17]. For wideband operation, monopole antennas have been widely used as implantable antennas in the open literature [16], [17].

In order to meet the demands for biodegradable and biocompatible biomaterial for the manufacture of an implantable antenna, innovation must deliver a serious replacement for the petroleum-based counterparts. This innovation seems to be driven by the recent advances in the research and development of bio-based materials derived from biomass processing. Biomass conversion to biomolecular precursors is most efficiently accomplished via thermochemical decomposition

consisting of three primary methods: chemical hydrolysis, gasification, and pyrolysis. Hydrolysis methods are typically used to separate desirable biomass sugars from less desirable celluloses and lignin. Gasification and pyrolysis are both a thermal decomposition of biomass. Gasification occurs at a temperature range between 500 °C – 1700 °C, with controlled oxygen, which converts bio-char into volatiles. Pyrolysis occurs at a lower temperature range between 200 °C – 750°C, in an inert environment, and produces less synthesis gas (SYNGAS) and more char than gasification [22]. Pyrolysis is broken down into fast and slow pyrolysis, indicated by a difference in heating rate. Three major products of biomass pyrolysis are obtained: volatiles (vapor), bio-oils (liquid), and bio-char (solid). Bio-oils are easily separated into two subcategories, light bio-oils and tars. The light bio-oils have been investigated thoroughly [23], [24], which often includes mitigation of tar [25], because it is the most valuable. Minimal to no work, however, has been conducted on utilizing the tar byproduct for the production of low-volume, high-value biomaterials for device manufacturing.

In this study, a biomass composition of sunflower seed shells (SSS) and sugar beet pulp (SBP) shreds were thermochemically processed into high quality biocarbon substrate by slow pyrolysis. SSS substrate was added in composite with poly lactic acid (PLA), a biodegradable, and biocompatible commercial polymer. The overarching objective of this research is determining if the substrate produced from SSS or SBP will yield the same desirable characteristics as PLA has for medical applications. To achieve the stated objective, we synthesized the desired biocarbon substrates in purified forms and in composites. Produced substrates were characterized and their chemical, electronic and mechanical properties fully quantified. After which, an antenna module was designed and fabricated using the produced biomaterial. Numerical investigations of the design were performed to guide the design and validate the methodology. To demonstrate the applicability of the proposed material for sensing applications, an antenna was designed and simulated and experimentally tested while placed under high permittivity materials such as soil, water, and muscle tissue phantom. Numerical investigations were carried out using ANSYS HFSS software (HFSS) [26]. The communication link of the antenna was measured in free space and through muscle tissue phantom for different distances.

II. EXPERIMENTAL

A. SUBSTRATE RECOVERY

SSS were supplied by CHS Sunflower, Grandin, ND. SBP was supplied by American Crystal Sugar Company, East Grand Forks, MN. The biomasses were dried then pyrolized in a Thermolyne 21100 tube furnace reactor at temperatures ranging from 350°C to 600°C. Figure 1 depicts the pyrolysis reactor set up. A stainless steel reactor with flanges on both sides was used. One side was rigged with a gas line inlet, the other had a nozzle for product to be recovered. This semi-batch process consisted of loading biomass into the

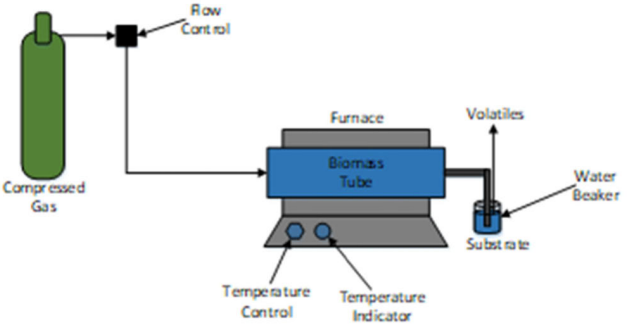

FIGURE 1. Experimental pyrolysis reactor set-up and configuration.

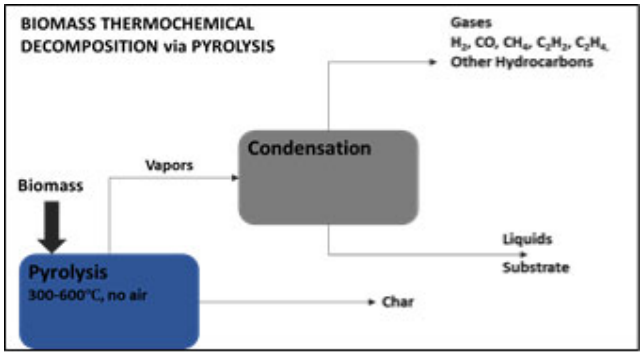

FIGURE 2. Functional block flow diagram of biomass pyrolysis process.

reactor, and feeding argon gas to displace oxygen within the system. Sample sizes for each trial were 50 g of biomass. The reactor was set to heat at 15°C min-1 until the desired temperature was reached, then allowed to slowly cool to room temperature. The substrate was directly captured into a beaker of water.

Figure 2 depicts a functional schematic of the pyrolysis process. The substrate samples are to be denoted as sunflower carbon substrate (SCS), and pulp carbon substrate (PSC). Char is a major product that has potential to be used as an activated carbon material, with multiple applications in environmental protection and energy storage [27]. SSS char samples were recovered and are to be denoted as sunflower shell char (SSC). Char and substrate recovery values were recorded, volatile and oil values were calculated by difference. The recovered substrate was dried in a vacuum oven before testing was conducted.

Acid treatments with hydrochloric acid (HCl) and base treatments with sodium hydroxide (NaOH) were applied to the SSS biomass to investigate the effects on carbon substrate recovery. Raw SSS were soaked in 1 Molar HCl for acid treatments and 1 Molar NaOH for base treatments for approximately one hour at room temperature, under constant stirring. The treated SSS was then dried in an oven for another hour. The treated and dried SSS were then pyrolized at 400 °C, and the substrate and char yields were calculated according to (1).

$$Yield = \frac{Recovered\ Product\ Weight}{Initial\ Sample\ Weight} \times 100 \qquad (1)$$

B. CHEMICAL ANALYSIS

Multiple chemical analyses were performed to better understand the chemical make-up of the SCS compared to SSS. Biomass is composed of three major chemical components: cellulose, hemicellulose, and lignin. Although there are conflicting ideas about the exact chemical makeup of pyrolysis tar [28], it is well agreed that this matter is largely comprised of aromatic compounds and ethers. Some reasons for the disagreement are the chemical make-up of tar is highly dependent on the biomass precursor and reaction conditions [29]. At higher pyrolysis temperatures, the substrate is broken down from oxygenated compounds into lighter hydrocarbons. Slow heating rates can have the opposite effect due to the low residence time of tar in the reactor. Nonetheless, this research is focused on recovering the substrate at lower temperatures when the yields are the highest; and there are oxygenates, ethers and phenols present in the material, considering the positive impact these functional groups traditionally have on electrical properties [30].

Proximate and Ultimate analysis were performed on SSS, SSC, and SCS products from the pyrolysis reaction. Proximate analysis was performed using a thermogravimetric analysis with differential scanning calorimetry (TGA/DSC) method with a SDT Q-600 analyzer. Samples were heated at a rate of 15°C min-1 in an N2, or air atmosphere. A CHN elemental analysis was conducted by Atlantic Microlab Inc., Norcross, GA.

Functional groups of the SCS were determined using a ThermoNicolet NEXUS 460 FTIR equipped with a ZnSe crystal and DTGS detector. The samples were tested in attenuated total reflection mode with a resolution of 4 cm-1 and 16 scans per sample.

Water absorption tests for the substrate were also recorded using ASTM D570. In this standard, a dry sample with a known weight is placed in distilled water over a desired amount of time. The samples are weighed before and after being placed in water and the percent water absorption is calculated according to (2).

$$Water\ Absorption\% = \frac{Wet\ Weight - Dry\ Weight}{Dry\ Weight} \times 100 \tag{2}$$

C. ELECTROMAGNETIC TESTING

The parameter that describes the propagation of electromagnetic radiation within materials is complex permittivity. Permittivity is related to other physical properties such as temperature, density, and water content. Low-water-content materials, such human skin and fat tissue or dry soil, have permittivity values that are estimated to be less than half those of high-water-content tissues such as blood tissue or wet soil. Increase of water content can also increase the dispersive characteristics of dielectric properties. In general, complex permittivity (ε) is expressed as:

$$\varepsilon = \varepsilon'(\omega) - j\varepsilon''(\omega) = \varepsilon_r \varepsilon_0 (1 - jtan\delta_e) \tag{3}$$

where ω is the angular frequency, ε' is the real part of complex permittivity and is related to the free-space permittivity ($\varepsilon_0 = 8.85 \times 10^{-12}$ F/m) by dielectric constant ε_r. ε'' is the imaginary part of complex permittivity that can also be shown by loss tangent ($\tan\delta_e$). Loss tangent shows the material losses and can be written as $\varepsilon'/\varepsilon''$. The frequency variations of the real and imaginary parts of complex permittivity are not independent and they are connected via the Kramers–Krönig relationship.

These properties were measured for dried SCS and composites. The method of measurement was using a Keysight High Performance Dielectric Probe 85070E attached to a Keysight 85107B Vector Netowork Analyzer (VNA). The measurements were performed at room temperature. Based on the material measurements a simple antenna was designed and fabricated to examine the material performance as a substrate material for RF planar antennas.

D. MECHANICAL TESTING

Mechanical properties of the developed materials were conducted using a Hysitron Ubi-1 Nanoindenter (with peak load capacity of 10 mN) which is a quasistatic depth-sensing indentation system for nanomechanical testing of Young's modulus, hardness, and fracture toughness. It is a great tool for measuring mechanical properties of materials of small volume such as coatings and thin films as well as soft materials. Assessing the mechanical properties through instrumented indentation is progressively growing due to its impending advantages over the conventional uniaxial tests. These advantages include small specimen volume, nondestructive nature, being a convenient and reliable testing method, and the capability to characterize local mechanical properties of heterogeneous materials [31].

A self-similar pyramidal Berkovich indenter was used in this study which is a common indenter in small-scale indentation studies. The face angle of the Berkovich indenter normally used for nanoindentation testing is 65.27°, which gives the same projected area-to-depth ratio as the Vickers indenter. The tip radius for a typical new Berkovich indenter is on the order of 50–100 nm.

The methodology proposed by Oliver and Pharr [32] is currently the most widely used method for calculating hardness in nearly all of the commercial depth sensing indentation applications. The hardness value can be inferred from the P-h curve as follows:

$$H_{Q\&P} = \frac{P}{A_c} \tag{4}$$

$$S = \left.\frac{dP}{dh}\right|_{P=P_{max}} \tag{5}$$

$$h_c = h_{max} - \epsilon \frac{P_{max}}{S} \tag{6}$$

$$A_c = 24.5h_c^2 + \sum_{i=1}^{8} C_i h_c^{1/2^{i-1}} \tag{7}$$

where S is the "unloading stiffness" measured at the maximum penetration depth; ϵ is a geometrical constant and its

value depends on the type of indenter (for a conical indenter, $\epsilon = 2(\pi - 2)/\pi$. C_i are the constants which describe the deviations due to an indenter tip. Those constants are calibrated by fitting the relations between A_C and h_c of a known material. The process begins with the calculation of h_c and the projected contact area A_C can be determined as:

$$A_C = \frac{\pi S^2}{4E_r^2} \tag{8}$$

where E_r is the reduced modulus defined as:

$$\frac{1}{E_r} = \frac{1 - \upsilon^2}{E} + \frac{1 - \upsilon_i^2}{E_i} \tag{9}$$

In (8), E and E_i are elastic moduli of the indented material and of the indenter; υ and υi are Poisson's ratios of the indented material and indenter, respectively. For a diamond indenter, $E = 1140$ GPa and $\upsilon_i = 0.07$. Since E_i is nearly ten times larger than that of metals, the indenter can be considered a rigid body and the last part of (6) is assumed as zero. If we know the parameters of a known material, the reduced modulus E_r can be obtained from (8). Subsequently, the constants C_i in (6) can be calibrated from the experimental data gathered for this known material.

E. POLYMER COMPOSITE FABRICATION

Composite samples with PLA were made to manipulate the electronic and mechanical properties of the SCS. PolyPlus ™ PLA filaments were obtained from Polymaker Shanghai, CN. Composites at weight ratios of 0.5:1, 1:1, and 2:1 (PLA:SCS) were produced. Two techniques were investigated to produce the composites: 1) melting PLA at 210° C and mixing it with liquefied SCS at their respective weight ratios in a crucible, 2) dissolving the PLA filaments in tetrahydrofuran (THF) then mixing the dissolved PLA with liquefied SCS. Samples were heated and mixed several times to ensure homogeneity in the mixture. THF was removed by evaporation at 70 °C, for at least 6 hours, in an inert atmosphere to prevent degradation of the substrate. While the two techniques produced identical substrates, the second method achieved homogeneous mixtures with fewer heating steps and less mixing. Substrates used for antenna fabrication were molded into the desired dimensions on a Teflon sheet, and trimmed with a sharp razor blade for smooth edges. Samples were stored in a cool dry place prior to use.

III. RESULTS AND DISCUSSION

A. SUBSTRATE RECOVERY

Considering the pyrolysis temperature is an important factor in terms of product yield, the yields of each product were recorded as a function of temperature. SCS recovery levels peaked at 7.9 wt.% at reactor temperatures around 500°C. Substrate cracking was experienced at temperatures higher than 500°C, which was apparent since SCS and SSC recoveries decreased while volatile production increased. Figure 3 depicts the correlation of component recoveries at varied reactor temperatures, where Figure 3(a) contains the substrate yields, Figure 3(b) contains the char yields, and Figure 3(c) contains the oil and volatile yields which were calculated by difference. Substrate yields from sugar beet pulp pyrolysis are not shown, but had substantially lower yields than SCS, likely due to the weaker ether linkages in the raw sugar beet pulp resulting from significantly lower lignin content compared to SSS.

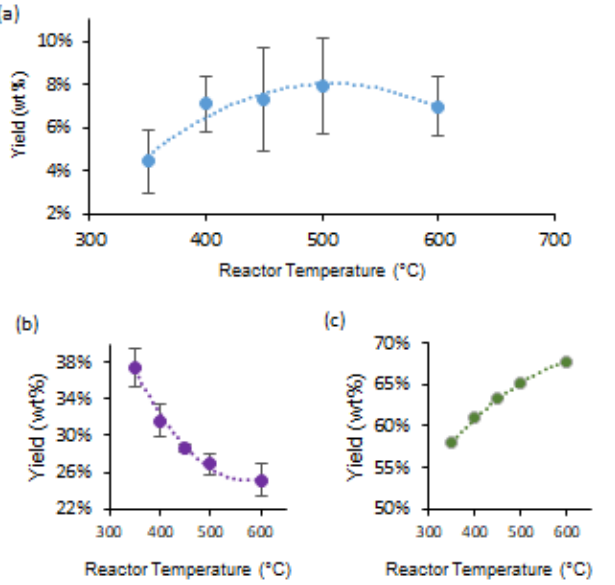

FIGURE 3. Sunflower shell pyrolysis product yields of (a) substrate, (b) char, and (c) oil and volatiles calculated by difference.

Acid and base treatments were performed to identify the effects the treatments have on pyrolysis product recoveries. Treated SSS samples were pyrolized at 400 °C. Neither acid nor base treatments had a positive impact on substrate recoveries. Acid treatments resulted in the lowest substrate recovery and the highest volatile yields, while base treatments had higher char recoveries.

It is important to note, that although the chemical, mechanical, and electromagnetic properties may be unique for each biomass under pyrolysis (SCS and sugar beet pulp), and acid/base treated SSS, yield is the most important factor considered for further analysis in this study. Only SCS was produced with sufficient yield in order to perform subsequent analysis and to fabricate RF antennas. Hence, SCS was chosen for further characterization and antenna fabrication.

B. CHEMICAL ANALYSIS

Multiple chemical analysis techniques were performed to quantify the chemical make-up of the SCS and SSC products, as well as assessing the pyrolysis process. Table 1 contains the results from a proximate analysis. All samples were tested after air drying for several days. Moisture content was averaged from TGA curves in both air and N2 atmospheres to reduce the possibility of noise caused by gas absorption into the sample. Ash contents were recorded while the TGA samples were in the presence of oxygen. Volatile contents

TABLE 1. Proximate analysis of sunflower shell and pyrolysis products.

Material	Moisture wt %	Ash wt %	Volatiles wt %	Fixed Carbon* wt %	C%	H%	N%	O%*
SSS	3.45	4.46	81.90	10.19	48.24	5.84	0.3	41.16
SCS	0.30	0.38	79.48	19.92	73.35	7.99	2.97	15.33
SSC	2.60	11.28	36.06	50.06	65.93	3.54	2	17.25

* Calculated by Difference

were recorded while the TGA samples in contact with inert gas. Fixed carbon content was calculated by difference [33].

The SSC retains mostly fixed carbons and volatiles, most of which removed at temperatures above 450 °C, this is also where tar cracking occurred in the pyrolysis reaction. The SCS consists primarily of volatiles, mostly removed between temperatures of 200 °C and 500 °C, this is the temperature range where substrate recovery was the highest. Fixed carbon makes up the remainder of the SCS, which does not degrade without the presence of a reactive gas due to strong bonding interactions. The most important component investigated in this analysis is the shift in fixed carbon, as this corresponds to strongly bonded aromatics and other pi bonded linking groups such as alkenes and alkynes which contribute to desirable electromagnetic properties. As expected, the fixed carbon increases in both products after pyrolysis of SSS, and is higher in the SSC compared to SCS.

Table 1 also includes the results from the ultimate elemental analysis. The analysis presents the amount of carbon, hydrogen and nitrogen in the samples. Oxygen is assumed to make up the remainder of the samples since sulfur and other chemical constituents in SSS are typically low [34]. The SCS and SSC products are primarily composed of carbon and oxygen. As expected, the carbon content in SCS and SSC samples were higher than in the SSS. Extrapolation of the results indicate the majority of oxygen and some hydrogen in the SSS leave the pyrolysis process as volatiles, while carbons and nitrogens remain in the SSC or are condensed as SCS. It is interesting to note that the SCS has a higher carbon content, but lower fixed carbon content that SSC. This is indicative of long chain carbon molecules present in the SCS and rigid carbon molecules in the SSC [35].

Figure 4 depicts the FTIR spectra for the SCS. Table 2 is an analysis of the curve and the typical compounds for each reading. The analysis was performed as outlined by Smith [36]. The strong signals in the spectra occurred at 2920 (asymmetric CH2), 2850 (symmetric CH2), 1700 (toluene rings), and 1200-1100 (ether stretching). The duplet peak between 1500 and 2000 indicates alkene groups. These peaks coupled with the duplet around 2950 are indicative of saturated alkene bonding. It is important to note that peaks

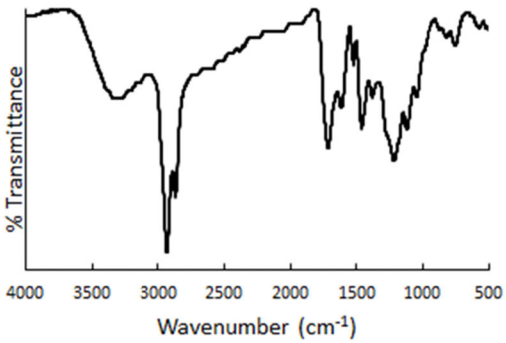

FIGURE 4. FTIR spectra of biocarbon substrate.

TABLE 2. FTIR analysis summary for biocarbon substrate.

Wavenumber[a]	Molecular Vibration	Functional Group
3300-3200 (m)	O-H Stretching	Alcohols
2920 (s)	C-H_2 Asymmetric	Alkyl, Aliphatic, Aromatic
2850 (s)	C-H_2 Symmetric	
1700 (s)	Toluene Ring Mode	Toluene
1600, 1450 (m)	Xylenes Ring Mode	Xylenes
1510 (w)	N-H Bends	Amines
1380 (w)	C=O Bends	Aldehydes
1200, 1100 (s)	C-O-C Ether Stretch	Aryl-Alkyl Ether Linkage Pyranose Ring
1030 (m)	C-H Bends	Aromatic Hydrogens
730 (w)	N-H Wag	Amines

[a] Signal: (s): strong, (m): moderate, (w): weak

between 1000 and 1200 were not attributed to functional groups containing sulfur, as the sulfur content was assumed negligible. These signals indicate the substrate is likely composed primarily of chained compounds with alkene and ether linkages, as well as aromatic toluene and xylenes.

Water absorption was quantified to be less than 0.5 % by mass. This indicates that the -OH stretching is probably not a result of water interference. It also allows some confidence that further electromagnetic/mechanical analysis is not influenced by water absorption into the samples.

C. ELECTROMAGNETIC ANALYSIS

Dielectric properties (i.e., complex permittivity $\varepsilon = \varepsilon' - j\varepsilon''$) of PLA, SCS, and composite materials were measured using Keysight 85070E high-performance dielectric probe. The two samples were tested for each material, and only one measurement is shown due to high similarity between replicates. The results in Figure 5 reveal the two base materials (PLA and SCS) had very different permittivity values. PLA was close to 1 while SCS was near 3.4 in much of the frequency range tested. As expected, the permittivity of composite samples fell between or near those of the base materials.

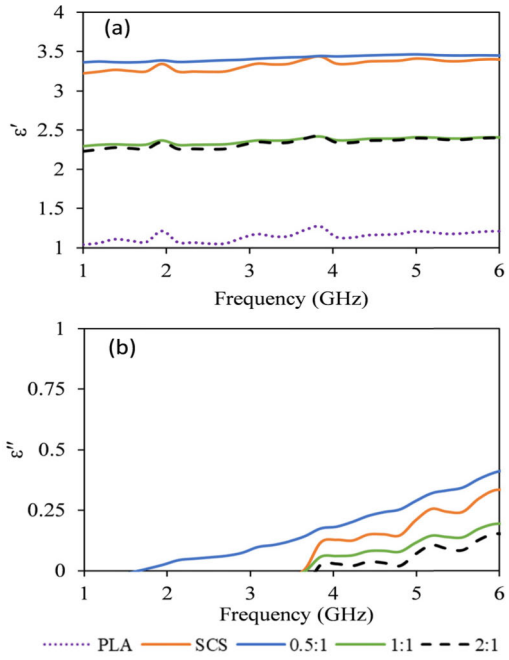

FIGURE 5. Permittivity measurements of base and composite materials (in terms of PLA:SCS); (a) dielectric constant (ε') and (b) dielectric loss factor (ε'').

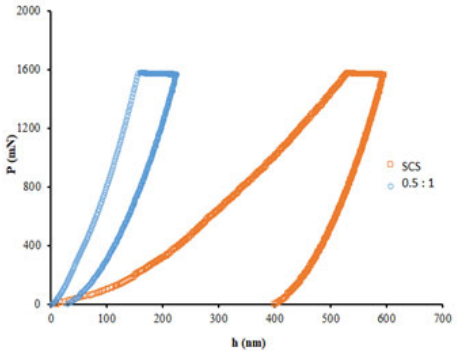

FIGURE 6. Load/displacement curves include three stages of loading, holding, and unloading.

TABLE 3. Mechanical properties of SCS and 0.5:1 composite material.

Property	SCS	0.5:1 PLA:SCS
Reduced Modulus (GPa)	0.42 ± 0.02	0.39 ± 0.09
Young's Modulus (GPa)	0.41 ± 0.02	0.35 ± 0.09
Hardness (MPa)	0.19 ± 0.02	0.98 ± 0.66

Composites of 1:1 and 2:1 PLA:SCS showed similar values, likely due to some imperfect mixing or phase separation when large amounts of PLA are present. However, in the composite with a majority SCS (0.5:1 PLA:SCS), the permittivity was reasonably the same as the SCS. This indicated that the small amount of PLA did not have any negative effect on SCS permittivity, but actually smoothed the results over the entire frequency range, indicated by a relatively straight line. Based on these permittivity results and the apparent improved mechanical performance, 0.5:1 PLA:SCS was determined to be the most appropriate composite for antenna fabrication.

D. MECHANICAL TESTING

To demonstrate the improved mechanical performance of the composite material, nano-indentation tests were conducted to record mechanical properties of the SCS and 0.5:1 PLA:SCS composite. Figure 6 shows load/displacement plots of both SCS and the composite specimen.

The pure SCS shows a viscoplastic behavior, meaning the deformation of the material follows a rate-dependent inelasticity. Stress strain behavior from indentation testing of viscoplastic material was examined by Huber *et al.* [37]. Having a more viscoplastic material is an important characteristic for some branches of bio-material science. For example, Charrier *et al.* observed the inelastic behavior in poplar cell walls and concluded that decreasing the elastic modulus could improve delignification which is an important step in overcoming recalcitrance [37].

As seen under a contact peak load of 1600 mN, the indenter runs deeper in the SCS sample as compared to the composite sample which shows that the composite sample is harder than the SCS. Indeed, the constituents in the composite material enhances the resistance against indentation in the matrix. In other words, the increase in microhardness values could be primarily attributed to the relatively uniform distribution of reinforcement phase and its higher constraint to the localized matrix deformation during indentation [38].

To further exemplify the improved mechanical properties, the reduced modulus, Young's modulus, and hardness were calculated according to equations 3-7 and listed in Table 3.

E. ANTENNA DESIGN

For testing purposes, monopole antenna was designed using the composite material (0.5:1 PLA:SCS) dielectric properties. Antennas are shown in Figure 7, along with the dimension details. Two samples of the substrate material were prepared with dimensions of 50 mm × 50 mm × 2 mm (i.e., length × width × thickness). Samples were then used in fabricating the monopole antenna, as shown in Figure 8. It is worth mentioning that the two antennas were fabricated to account for any measurement error sources that might occur during the fabrication or/and the measurement phases of the antenna.

Reflection coefficients (S_{11}) of the fabricated antennas were measured in free-space using Keysight E5071C vector network analyzer (300 kHz – 20 GHz frequency operating range). S_{11} parameter is used to determine the operating frequency range of the antenna (i.e., antenna bandwidth) and the resonance frequencies. The measurement setup and S_{11} results for antenna 2 are shown in Figures 8 and 9, respectively. Surface roughness and irregular geometry of sample 1 resulted in unreliable S_{11} measurements; hence, they were not

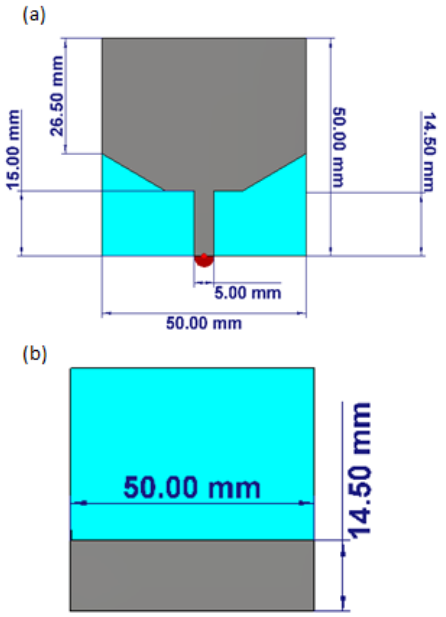

FIGURE 7. Monopole antenna dimensions (a) front, and (b) back views.

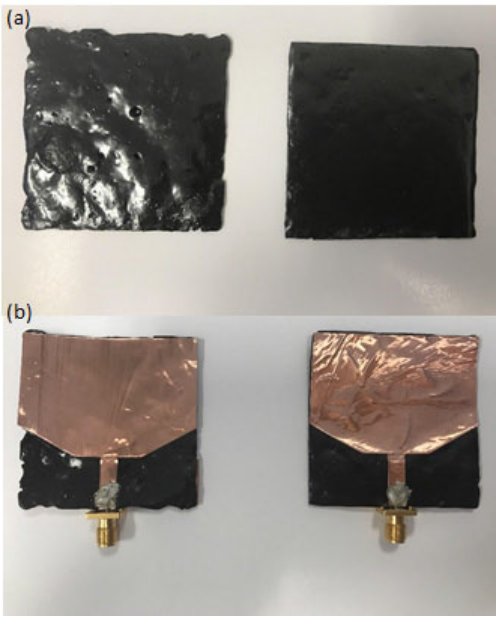

FIGURE 8. Substrate samples and fabricated monopole antennas.

reported. Numerical simulation (HFSS) results agreed fairly well with experimental values as depicted in Figure 9.

F. ANTENNA PERFORMANCE UNDER HIGH PERMITTIVITY MATERIALS

To demonstrate the use of sensors and antennas in biomedical and agricultural applications, they should be tested in the vicinity of materials that have similar dielectric properties to body tissues and soil, respectively. In biomedical applications, before *in vivo* testing the device, sometimes it is possible to do these testing on *ex vivo* tissue samples, but for more accurate testing it is better to use tissue mimicking

FIGURE 9. S_{11} measurement setup using E5071C vector network analyzer.

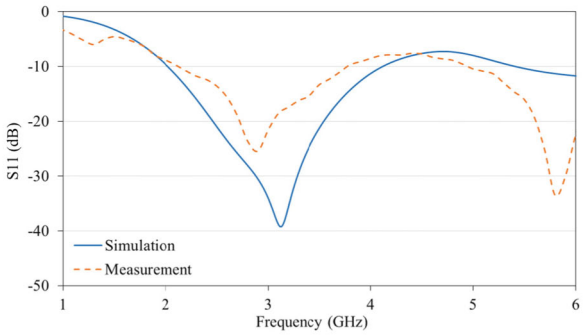

FIGURE 10. Simulated and measured S_{11} (reflection coefficient) of the fabricated antenna.

materials (phantoms). Phantoms are used as tissue substitutes. There are several databases that give the approximation of various tissue dielectric properties [39], however, note that these properties can vary due to various reasons such as temperature, water content, and physiological composition.

Some tissue-mimicking phantom materials developed are reviewed in [40]. Some phantoms are simply made of water and salt with various percentages. Some other phantoms are gelatin based. In most of cases phantoms should be used for a specific frequency that it mimics the tissue dielectric properties at that frequency. It is generally difficult to develop a phantom which matches the tissue in a wide frequency band [41].

To mimic the agricultural applications, reflection coefficient (S_{11}) of the fabricated antenna was measured when antenna was placed under a layer of water, and wet soil, as shown in Figure 11. Placing the antenna in different materials creates a loading effect that can be used for sensing the humidity of the material. A similar simulation model was created in HFSS. To include the insulating layer between antenna and water layer, 1 mm air gap was considered in simulation. Water dielectric properties considered in simulation were relative permittivity (dielectric constant) of 78 and conductivity of 1.5 S/m. Figure 11 compares the simulation and

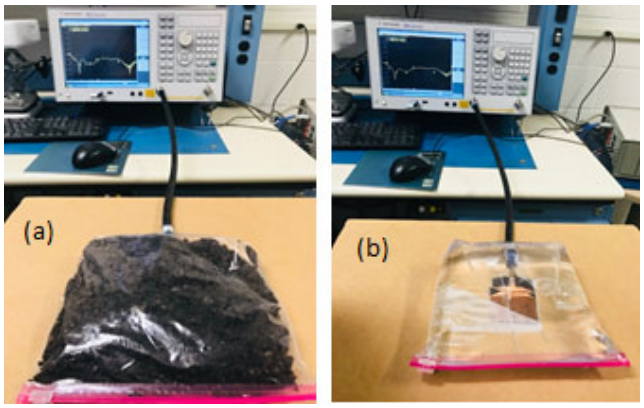

FIGURE 11. Antenna covered with (a) soil, and (b) water.

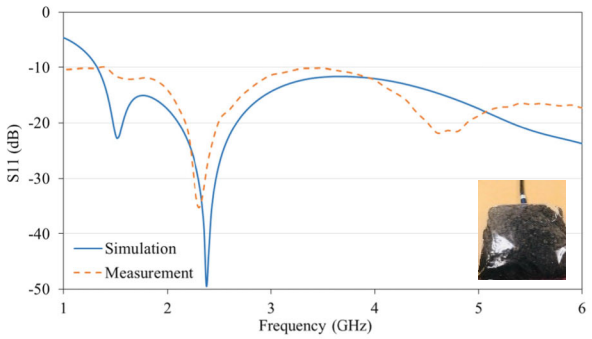

FIGURE 12. Simulated and measured S_{11} of the antenna under wet soil.

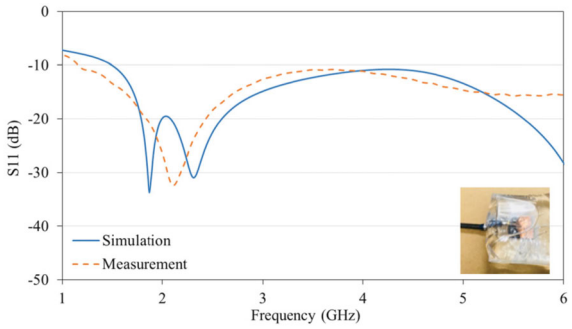

FIGURE 13. Simulated and measured S_{11} of the antenna under water.

measured results. Similar procedure was followed to measure wet soil. In HFSS simulations, dielectric constant and loss tangent of soil were assumed to be 13 and 0.29, respectively. Measured and simulated results are compared in Figure 12. To show and compare the change in the resonance frequency of the antenna in Figure 13 the measured values for free-space, under water and under soil are shown in one plot. With a mapping, the phenomena can be used to measure humidity of the material. It is worth mentioning that the dielectric constant of wet soil can vary between 10 and 20 [42]. The dispersive behavior of water also causes variation in water permittivity and conductivity at various frequencies. In these simulations we did not consider frequency dependency of covering material and estimated an average value for them.

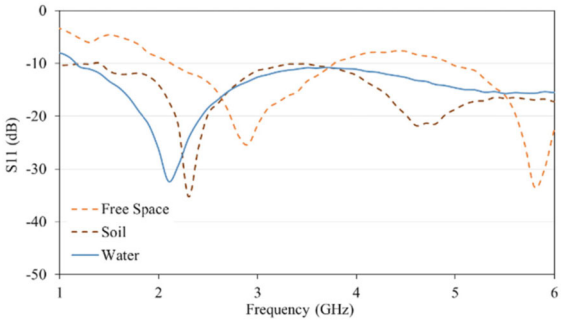

FIGURE 14. Comparison of measured S_{11} of the antenna in free-space, under wet soil, and under water.

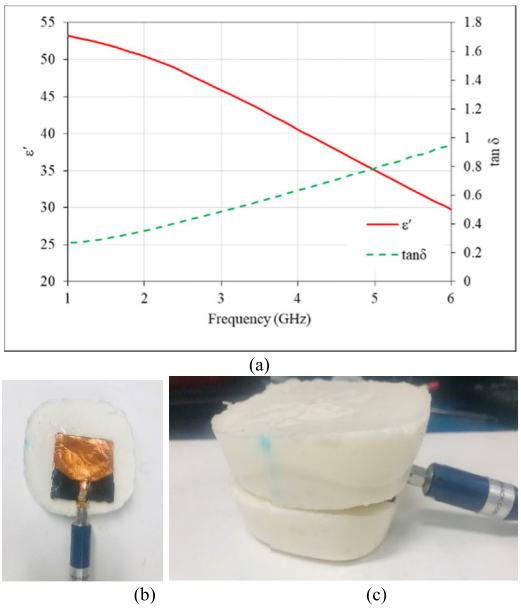

FIGURE 15. (a) Measured dielectric properties of phantom. Measurement setup for (b) wearable case, and (c) implanted case.

To examine the performance of the antenna in the wearable and implanted wireless devices a gelatin based muscle tissue phantom was prepared. The phantom was prepared based on the recipe provided in [43]. The dielectric properties of the muscle phantom were measured using Keysight High Performance Probe 85070-60010 and results are shown in Figure 14(a). Two cases of measurement and simulation were considered. For wearable applications (Figure 14(b)), the antenna was placed on a 2.5cm thick layer of phantom. For implanted applications, as shown in Figure 14(c), the antenna was placed between two layers of phantom material. Each layer had a thickness of 2.5 cm. Measured and simulated S_{11} for the wearable case is shown in Figure 15. The results for implanted case is shown in Figure 16. In HFSS simulations, the measured dielectric properties of the phantom were used to define a frequency dependent material. In the wearable case no spacing between the phantom and antenna's ground plane was considered, in the implanted case a 0.5 mm air-gap was considered as the insolation layer.

In a wireless communication scenario the link budget is important; therefore, the transmission coefficient (S_{21}) was

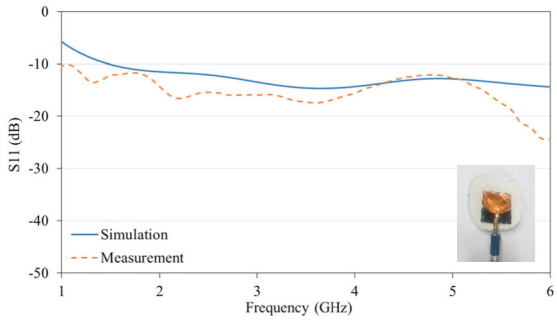

FIGURE 16. Simulated and measured S_{11} of the antenna on the muscle phantom.

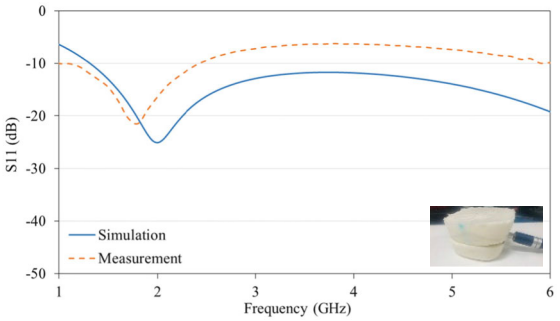

FIGURE 17. Simulated and measured S_{11} of the antenna implanted inside the muscle phantom.

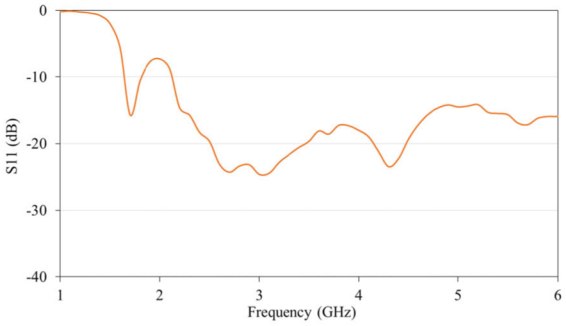

FIGURE 18. Measured S_{11} for the transmitting antenna used for link budget measurements.

measured using a directional double ridged horn antenna (2 GHz – 18 GHz A-info JXTXLB-20180) as a transmitter. Reflection coefficient of this antenna was measured and is shown in Figure 17. The measurement set up in free-space is shown in Figure 18 (a). The distance (d) between the antennas was changed from 20 cm to 50 cm and S_{21} was measured. The results are shown in Figure 18(b). As expected, the larger the distance between the antennas, the more losses in the communication link are observed, however, this loss is minimum at the resonance frequency.

Similar procedure and setup was used to measure S_{21} in the implanted and wearable cases. Three cases were considered, as shown in Figure 19(a)-(c). In the first case the antenna was implanted inside two layers of phantom of 2.5 cm thickness. In the second case, the antenna was moved under the two

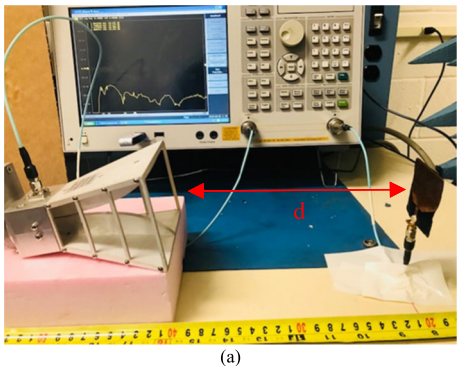

FIGURE 19. (a) Measurement setup for link budget (S_{21}), (b) measured S21 for various distances.

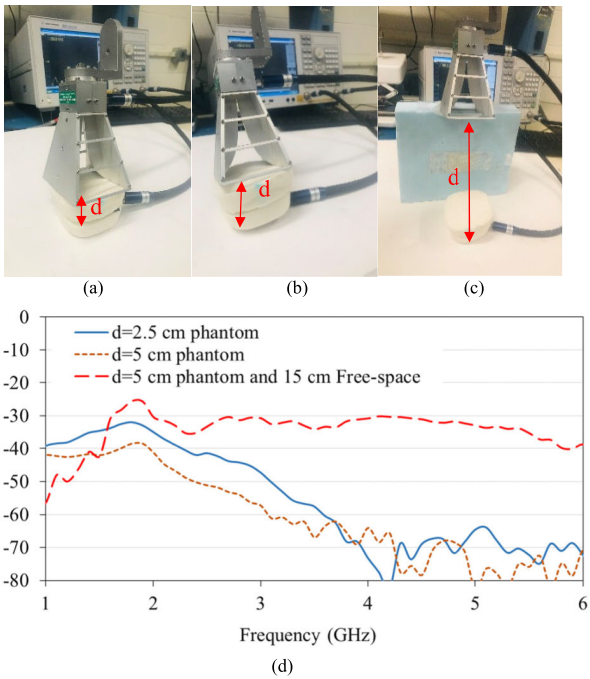

FIGURE 20. (a) Measurement setup for link budget (S21) (a) d = 2.5 cm phantom, (b) d = 5 cm phantom, (c) d = 15 cm frees-space and 5 cm phantom, (d) measurement results.

layers (5 cm of phantom on top). In the 3rd case the horn antenna was moved away from the top surface of phantom by 15 cm. The results of measurements are shown in Figure 19(d). The results show that the performance is better if the horn is moved away from the phantom. This is expected

as the horn antenna is designed to operate in free-space. The level of S_{21} is reasonable for this case, even when the antenna is under 5 cm of lossy tissue.

IV. CONCLUSION

The SCS is largely made up of volatile and fixed carbons. Infrared spectroscopy indicates the substrate is made up of CH2, toluene and xylene aromatic ring, and ether functional groups. The formation of these groups are likely in the form of small chain hydrocarbons with alkene and ether linkages as well as aromatic compounds. Adding the SCS in composite with PLA showed that dielectric and mechanical properties of the material can be manipulated. Mechanical properties of the material significantly increased while the low dielectric constant of PLA decreased the dielectric constant of the material. Further mechanical testing at varied temperatures should be conducted. Electronic tests with other materials in composite should also be conducted in order to manipulate an increase in the materials dielectric constant. An advanced chemical analysis should also be conducted in order to identify a more accurate understanding of the substrates molecular make up. Manipulation of mechanical, electronic, and chemical properties is important for the material to be implemented in RF sensor designs for agricultural or medical applications. This work has shown bio-waste material can be converted into products that have unique characteristics and have properties that can be manipulated to more desirable conditions.

REFERENCES

[1] C. H. Lee, H. Kim, D. V. Harburg, G. Park, Y. Ma, T. Pan, J. S. Kim, N. Y. Lee, B. H. Kim, K.-I. Jang, S.-K. Kang, Y. Huang, J. Kim, K.-M. Lee, C. Leal, and J. A. Rogers, "Biological lipid membranes for on-demand, wireless drug delivery from thin, bioresorbable electronic implants," *NPG Asia Mater.*, vol. 7, no. 11, p. e227, 2015. doi: 10.1038/am.2015.114.

[2] K. J. Yu *et al.*, "Bioresorbable silicon electronics for transient spatiotemporal mapping of electrical activity from the cerebral cortex," *Nature Mater.*, vol. 15, no. 7, pp. 782–791, 2016. doi: 10.1038/nmat4624.

[3] S.-K. Kang *et al.*, "Bioresorbable silicon electronic sensors for the brain," *Nature*, vol. 530, pp. 71–76, Jan. 2016. doi: 10.1038/nature16492.

[4] R. Li, L. Wang, D. Kong, and L. Yin, "Recent progress on biodegradable materials and transient electronics," *Bioactive Mater.*, vol. 3, no. 3, pp. 322–333, 2018. doi: 10.1016/j.bioactmat.2017.12.001.

[5] Y. Chen, Q. Zhang, A. Alomainy, P. S. Anwar, and L. Huang, "Characterizing physically transient antennas," *IEEE Trans. Antennas Propag.*, vol. 63, no. 6, pp. 2421–2429, Jun. 2015. doi: 10.1109/TAP.2015.2414444.

[6] L. S. Y. Wong, S. Hossain, A. Ta, J. Edvinsson, D. H. Rivas, and H. Naas, "A very low-power CMOS mixed-signal IC for implantable pacemaker applications," *IEEE J. Solid-State Circuits*, vol. 39, no. 12, pp. 2446–2456, Dec. 2004. doi: 10.1109/JSSC.2004.837027.

[7] J. A. Warren, R. D. Dreher, R. V. Jaworski, J. J. Putzke, and R. J. Russie, "Implantable cardioverter defibrillators," *Proc. IEEE*, vol. 84, no. 3, pp. 468–479, Mar. 1996. doi: 10.1109/5.486748.

[8] R. Bashirullah, W. Liu, Y. Ji, A. Kendir, M. Sivaprakasam, G. Wang, and B. Pundi, "A smart bi-directional telemetry unit for retinal prosthetic device," in *Proc. Int. Symp. Circuits Syst.*, vol. 5, May 2003, pp. 1–4. doi: 10.1109/ISCAS.2003.1206158.

[9] K. D. Wise, A. M. Sodagar, Y. Yao, M. N. Gulari, G. E. Perlin, and K. Najafi, "Microelectrodes, microelectronics, and implantable neural microsystems," *Proc. IEEE*, vol. 96, no. 7, pp. 1184–1202, Jul. 2008. doi: 10.1109/JPROC.2008.922564.

[10] A. Moglia, A. Menciassi, and P. Dario, "Recent patents on wireless capsule endoscopy," *Recent Patents Biomed. Eng.*, vol. 1, no. 1, pp. 24–33, 2008.

[11] R. Bashirullah, "Wireless implants," *IEEE Microw. Mag.*, vol. 11, no. 7, pp. S14–S23, Dec. 2010. doi: 10.1109/MMM.2010.938579.

[12] C. M. Boutry, A. Nguyen, Q. O. Lawal, A. Chortos, S. Rondeau-Gagné, and Z. Bao, "A sensitive and biodegradable pressure sensor array for cardiovascular monitoring," *Adv. Mater.*, vol. 27, no. 43, pp. 6954–6961, 2015. doi: 10.1002/adma.201502535.

[13] M. Luo, A. W. Martinez, C. Song, F. Herrault, and M. G. Allen, "A microfabricated wireless RF pressure sensor made completely of biodegradable materials," *J. Microelectromech. Syst.*, vol. 23, no. 1, pp. 4–13, Feb. 2014. doi: 10.1109/JMEMS.2013.2290111.

[14] D. Girbau, A. Ramos, A. Lazaro, S. Rima, and R. Villarino, "Passive wireless temperature sensor based on time-coded UWB chipless RFID tags," *IEEE Trans. Microw. Theory Techn.*, vol. 60, no. 11, pp. 3623–3632, Nov. 2012. doi: 10.1109/TMTT.2012.2213838.

[15] J. Yao, F. M. Tchafa, A. Jain, S. Tjuatja, and H. Huang, "Far-field interrogation of microstrip patch antenna for temperature sensing without electronics," *IEEE Sensors J.*, vol. 16, no. 19, pp. 7053–7060, Oct. 2016. doi: 10.1109/JSEN.2016.2597739.

[16] S. Kumar, T. Shanmuganantham, and G. Sasikala, "Design and development of implantable CPW fed monopole U slot antenna at 2.45 GHz ISM band for biomedical applications," *Microw. Opt. Technol. Lett.*, vol. 57, no. 7, pp. 1604–1608, 2015.

[17] H. Bahrami, S. A. Mirbozorgi, R. Ameli, L. A. Rusch, and B. Gosselin, "Flexible, polarization-diverse UWB antennas for implantable neural recording systems," *IEEE Trans. Biomed. Circuits Syst.*, vol. 10, no. 1, pp. 38–48, Feb. 2016.

[18] T. Homsai, C. Phongcharoenpanich, and W. Sriseubsai, "Bio-degradable material realization for antenna fabrication in wireless communications," in *Proc. MATEC Web Conf.*, vol. 192, 2018, Art. no. 01035.

[19] X. Huang, Y. Liu, S.-W. Hwang, S.-K. Kang, D. Patnaik, J. F. Cortes, and J. A. Rogers, "Biodegradable materials for multilayer transient printed circuit board," *Adv. Mater.*, vol. 26, pp. 7371–7377, Nov. 2014.

[20] H. Tao, M. A. Brenckle, M. Yang, J. Zhang, M. Liu, S. M. Siebert, R. D. Averitt, M. S. Mannoor, M. C. McAlpine, J. A. Rogers, D. L. Kaplan, and F. G. Omenetto, "Silk-based conformal, adhesive, edible food sensors," *Adv. Mater.*, vol. 24, no. 8, pp. 1067–1072, 2012.

[21] S. Yun, K. Kim, and S. Nam, "Outer-wall loop antenna for ultrawideband capsule endoscope system," *IEEE Antennas Wireless Propag. Lett.*, vol. 9, pp. 1135–1138, 2010. doi: 10.1109/LAWP.2010.2094996.

[22] *Global Syngas Technologies Council. Gasification vs. Pyrolysis*. Accessed: May 5, 2018. [Online]. Available: https://www.globalsyngas.org/applications/gasification-vs.-pyrolysis/

[23] D. Carpenter, T. L. Westover, S. Czernik, and W. Jablonski, "Biomass feedstocks for renewable fuel production: A review of the impacts of feedstock and pretreatment on the yield and product distribution of fast pyrolysis bio-oils and vapors," *Green Chem.*, vol. 16, pp. 384–406, Nov. 2014. doi: 10.1039/C3GC41631C.

[24] A. Oasmaa, B. Beld, P. Saari, D. C. Elliott, and Y. Solantausta, "Norms, standards, and legislation for fast pyrolysis bio-oils from lignocellulosic biomass," *Energy Fuels*, vol. 29, no. 4, pp. 2471–2484, 2015. doi: 10.1021/acs.energyfuels.5b00026.

[25] J. Han and H. Kim, "The reduction and control technology of tar during biomass gasification/pyrolysis: An overview," *Renew. Sustain. Energy Rev.*, vol. 12, no. 2, pp. 397–416, 2008. doi: 10.1016/j.rser.2006.07.015.

[26] *ANSYS HFSS*. Accessed: Aug. 2018. [Online]. Available: https://www.ansys.com/products/electronics/ansys-hfss

[27] X.-F. Tan, S.-B. Liu, Y.-G. Liu, Y.-L. Gu, G.-M. Zeng, X.-J. Hu, X. Wang, S.-H. Liu, and L.-H. Jiang, "Biochar as potential sustainable precursors for activated carbon production: Multiple applications in environmental protection and energy storage," *Bioresource Technol.* vol. 227, pp. 359–372, Mar. 2017. doi: 10.1016/j.biortech.2016.12.083.

[28] K. Maniatis and A. A. C. M. Beenackers, "Tar protocols. IEA bioenergy gasification task," *Biomass Bioenergy*, vol. 18, no. 1, pp. 1–4, 2000. doi: 10.1016/S0961-9534(99)00072-0.

[29] T. A. Milne, R. J. Evans, and N. Abatzaglou, "Biomass gasifier 'tars': Their nature, formation, and conversion," Nat. Renew. Energy Lab., Golden, CO, USA, Tech. Rep. NREL/TP-570-25357, 1998.

[30] H. Inokuchi and H. Akamatu, "Electrical conductivity of organic semiconductors," *Solid State Phys.*, vol. 12, pp. 93–148, Jan. 1961. doi: 10.1016/S0081-1947(08)60653-0.

[31] W. C. Guo, H. Xu, X. Q. Gao, X. L. Hou, and Y. Li, "A modified method for hardness determination from nanoindentation experiments with imperfect indenters," *Adv. Mater. Sci. Eng.*, vol. 2016, Nov. 2016, Art. no. 9213841. doi: 10.1155/2016/9213841.

[32] W. C. Oliver and G. M. Pharr, "An improved technique for determining hardness and elastic modulus using load and displacement sensing indentation experiments," *J. Mater. Res.*, vol. 7, no. 6, pp. 1564–1583, 1992. doi: 10.1557/JMR.1992.1564.
[33] K. Annamalai, J. Sweeten, and S. Ramalingam, "Technical notes: Estimation of gross heating values of biomass fuels," *Trans ASAE*, vol. 30, no. 4, pp. 1205–1208, 1987. doi: 10.13031/2013.30545.
[34] S. Seetharaman, J. Subramanian, K. S. Tun, A. S. Hamouda, and M. Gupta, "Synthesis and characterization of nano boron nitride reinforced magnesium composites produced by the microwave sintering method," *Materials*, vol. 6, no. 5, pp. 1940–1955, 2013. doi: 10.3390/ma6051940.
[35] *ECN Phylllis 2 Sunflower Seed Shells*. Accessed: Apr. 30, 2018. [Online]. Available: https://www.ecn.nl/phyllis2/Biomass/View/878
[36] B. C. Smith, *Infrared Spectral Interpretation: A Systematic Approach*. Boca Raton, FL, USA: CRC Press, 1998.
[37] N. Huber, E. Tyulyukovskiy, H.-C. Schneider, R. Rolli, and M. Weick, "An indentation system for determination of viscoplastic stress–strain behavior of small metal volumes before and after irradiation," *J. Nucl. Mater.*, vol. 377, no. 2, pp. 352–358, 2008. doi: 10.1016/j.jnucmat.2008.03.013.
[38] A. M. Charrier, A. L. Lereu, R. H. Farahi, B. H. Davison, and A. Passian, "Nanometrology of biomass for bioenergy: The role of atomic force microscopy and spectroscopy in plant cell characterization," *Frontiers Energy Res.*, vol. 6, p. 11, Mar. 2018. doi: 10.3389/fenrg.2018.00011.
[39] S. Gabriely, R. Lau, and C. Gabriel, "The dielectric properties of biological tissues: II. Measurements in the frequency range 10 Hz to 20 GHz," *Phys. Med. Biol.*, vol. 41, no. 11, pp. 2251–2269, 1996.
[40] M. Lazebnik, E. L. Madsen, G. R. Frank, and S. C. Hagness, "Tissue-mimicking phantom materials for narrowband and ultrawideband microwave applications," *Phys. Med. Biol.*, vol. 50, no. 18, pp. 4245–4258, 2005.
[41] C. Hahn and S. Noghanian, "Heterogeneous breast phantom development for microwave imaging using regression models," *Int. J. Biomed. Imag.*, vol. 2012, Jan. 2012, Art. no. 803607. doi: 10.1155/2012/803607.
[42] A. Martinez and A. Brynes, "Modeling dielectric-constant values of geologic materials: An aid to ground-penetrating radar data collection and interpretation," *Bull. Kansas Geolog. Surv.*, vol. 247, 2001.
[43] T. Yilmaz, R. Foster, and Y. Hao, "Broadband tissue mimicking phantoms and a patch resonator for evaluating noninvasive monitoring of blood glucose levels," *IEEE Trans. Antennas Propag.*, vol. 62, no. 6, pp. 3064–3075, Jun. 2014.

AUSTIN TESSER received the B.S. degree in chemical engineering from the University of North Dakota, Grand Forks, ND, USA, in 2018. He is currently an Integrity Engineer with Lake Superior Consulting, Duluth, Minnesota.

ALA ALEMARYEEN received the B.Sc. degree from Mutah University, Jordan, in 2012, and the M.Sc. degree from the University of North Dakota (UND), USA, in 2015, where she is currently pursuing the Ph.D. degree, all in electrical engineering. Her current research interests include antenna theory and wave propagation, wearable and implantable antennas, and wireless communications.

JEREMY LEWIS received the B.S. degree from California State Polytechnic University Pomona, Pomona, CA, USA, in 2017, and the M.S. degree from the University of North Dakota, Grand Forks, ND, USA, in 2019, both in chemical engineering. He is currently a Postmasters Researcher with Los Alamos National Laboratory, Materials Physics and Applications Group, Materials Synthesis and Integrated Devices Division. His research interests include biomass pyrolysis, composite materials, mixed matrix membranes, and carbon membranes.

ALI ALSHAMI received the B.S., M.S., and Ph.D. degrees from Washington State University, Pullman, WA, USA, in 1997, 2001, and 2007, respectively. From 1997 to 1998, he was an Application Engineer with Canon USA Inc. From 2000 to 2003, he was a Technology and Development Engineer with Eaton/Cutler-Hammer Corporation. From 2006 to 2010, he was an Engineer and a Service Manager with Pace International, Valent BioSciences. He served as an Assistant Professor for the King Fahd University of Petroleum and Minerals (KFUPM), from 2010 to 2014. He is currently an Assistant Professor with the Department of Chemical Engineering, University of North Dakota. His research interests include biomaterials and bimolecular engineering, biochemical process engineering, bioseparation engineering, membrane separation processes, and process development and design.

MEYSAM HAGHSHENAS received the M.S. degree in materials and metallurgical engineering from the University of Tehran, Tehran, Iran, in 2006, and the Ph.D. degree in mechanical and materials engineering from the Water Institute, University of Waterloo, Waterloo, ON, Canada, in 2013. From 2009 to 2012, he was a Research and Development Engineer with Transform Automotive. From 2013 to 2015, he was a Lecturer and a Welding Engineer with the University of Waterloo. From 2014 to 2015, he served as a Project and Design Engineer/Metallurgist at Linamar Corporation. Since 2016, he has been an Assistant Professor with the Department of Mechanical Engineering, University of North Dakota. His research interests include material characterization, mechanical behavior of materials, and materials microstructure.

SIMA NOGHANIAN (M'03–SM'05) received the M.Sc. and Ph.D. degrees in electrical engineering from the University of Manitoba, Winnipeg, MB, Canada, in 1996 and 2001, respectively. From 2002 to 2003, she was an Assistant Professor with the Department of Electrical Engineering, Sharif University of Technology, Tehran, Iran. From 2003 to 2008, she was an Assistant Professor with the Department of Electrical and Computer Engineering, University of Manitoba. From 2008 to 2018, she was an Assistant Professor and an Associate Professor with the Department of Electrical Engineering, University of North Dakota, Grand Forks, ND, USA. She was a Visiting Professor with San Diego State University, San Diego, CA, USA, in 2018. She is currently an Electromagnetic Application Engineer with Phoenix Analysis and Design Technologies (PADT), Inc. Her current research interests include antenna design and modeling, flexible, 3D printed and wearable antennas, wireless power transfer, and microwave imaging. She is currently an Associate Editor of the following journals: the IEEE Antennas and Wireless Propagation Letters, the *IEEE Antenna Magazine*, *IET Microwaves, Antennas & Propagation*, *Applied Computational Electromagnetics Society Journal*, and *AEU—International Journal of Electronics and Communications*.